Int. J. Electrochem. Sci., 7 **(2012)** 11641 - 11654

International Journal of
ELECTROCHEMICAL
SCIENCE
www.electrochemsci.org

Recurrence and Nonlinear System Dynamic Analysis of the Electrochemical Oscillations Recorded in the System Mild Steel/H_3PO_4

G.A. Vázquez-Coutiño[1,2], *M. Palomar-Pardavé*[1,*], *M. Romero-Romo*[1], *H. Herrera-Hernández*[1], *M.T. Ramírez-Silva*[2]

[1] Universidad Autónoma Metropolitana-Azcapotzalco. Departamento de Materiales, Av. San Pablo 180. CP. 02200, México D.F. México.
[2] Universidad Autónoma Metropolitana-Iztapalapa. Departamento de Química, San Rafael Atlixco No.186 Col. Vicentina, C.P. 09340 México D.F., México.
[*]E-mail: mepp@correo.azc.uam.mx

Received: 12 October 2012 / *Accepted:* 8 November 2012 / *Published:* 1 December 2012

After formation of $FePO_4{:}2H_2O_{(c)}$ layer on the steel electrode by imposing a positive potential value; either potentiodynamic (anodic scan of a cyclic votammetry experiment) or potentiostatic (first potential pulse of a double potential step technique), during the reverse potential scan or the second potential step in the cathodic direction current oscillations were clearly noted in the interval from 530 to 300 mV. Electrochemical oscillations recorded, were analyzed using recurrence and nonlinear system dynamical analysis. From the estimation of different parameters: Lyapunov exponent, correlation dimension and spatiotemporal entropy, the presence of a chaotic behavior for this system has been found out.

Keywords: A. Mild steel; A. H_3PO_4; B. Cyclic voltammetry; B. Potentiostatic; C. Anodic films; C. Pourbaix diagram

1. INTRODUCTION

Electrochemical oscillations on both current [1-4] and potential [5-11] of different systems, namely: Fe/H_3P0_4 [1,7,8], Cu/ H_3P0_4 [2] , Ni/Ni(II) [3], Ag(001)/ Ag(I) [4], Stainless steel/ H_2SO_4, CrO_3 [5], Cu/Cu(II) [6], Zn/Zn(II) [9], Fe/NaCl [10,11] have been observed, most of them during the metal electrodissolution process. In particular, those reported by Ishihara and Asakura [8] related with the system Fe/H_3PO_4, H_2O_2 has been utilized to propose a thermal sensor. However, hitherto, to our acknowledge, electrochemical oscillations in the system mild steel (AISI SAI 1045) / H_3P0_4 has not

been reported and/or characterized, therefore in this work, from recurrence and nonlinear system dynamical analysis, the electrochemical oscillations recorded in this system is presented.

2. EXPERIMENTAL PROCEDURE

Experiments were carried out in a three compartment cell, which contained 20 mL of concentrate H_3PO_4 solution. All potentials reported in this study are quoted with respect to a Ag/AgCl (KCl sat) reference electrode. The counter electrode was a platinum wire of about 1 cm^2 surface area. Samples of mild steel (SAE 1045) were used as working electrodes. The working electrode was wet polished by 180, 300, 400, 600, 1200, 1500 grit polishing papers. After the polishing, it was washed with deionized H_2O and placed into the solution in a downward facing position. Tests were done at room temperature and under static conditions. The experimental apparatus used in this work for the determination of the cyclic voltammograms (CVs), as well as the double potential step chronoamperograms, was a potentiostat (PAR, 273) used to control the potential (E) of the working electrode.

3. RESULTS AND DISCUSSIONS

3.1 Thermodynamic analysis of the system

Considering that oxidation of steel immersed in the H_3PO_4 aqueous solution involves a multicomponent and multireactive system in which acid-base (proton, H^+, exchange) and complexation reactions may occur along with charge, e^-, transfer.

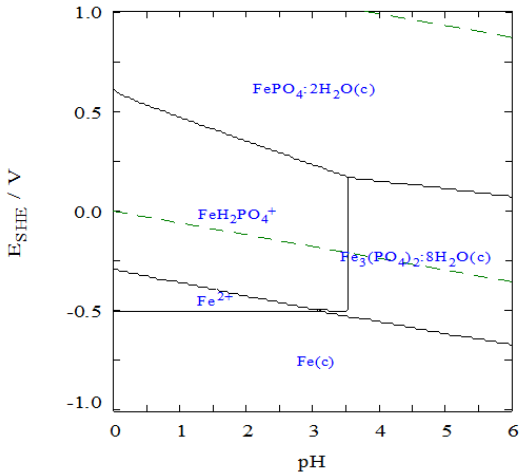

Figure 1. E-pH diagram constructed using the MEDUSA software [12] and considering the species and thermodynamic constants reported in Table 1, at constant temperature of 298 K, [Fe(II)] = 100 mM and $[PO_4^{3-}]$= 300 mM.

Table 1. Thermodynamic constants, 298 K, and the chemical species considered during construction of Figure 1 using the software MEDUSA and database HYDRA. The equilibria associated with the constants (K) are stated as follows: $wH^+ + xe^- + yFe^{2+} + zPO_4^{3-} \rightleftharpoons product$.

PRODUCT	Log K	REACTANTS			
		H^+	e^-	Fe^{2+}	PO_4^{3-}
Fe^{3+}	-13.02	0	-1	1	0
$Fe(OH)_2$	-20.80	-2	0	1	0
$Fe(OH)_3^-$	-33.40	-3	0	1	0
$Fe(OH)_4^{2-}$	-46.35	-4	0	1	0
$FeH_2PO_4^+$	22.25	2	0	1	1
$FeHPO_4$	15.95	1	0	1	1
$Fe(OH)^+$	-10.2	-1	0	1	0
$H_{2(g)}$	0.0	2	2	0	0
H_2O_2	-59.60	-2	-2	0	0
$H_2PO_4^-$	19.55	2	0	0	1
H_3PO_4	-21.70	3	0	0	1
HPO_3^{2-}	-4.09	3	2	0	1
HPO_4^{2-}	12.35	1	0	0	1
$O_{2(g)}$	-83.12	-4	-4	0	0
$O_{3(g)}$	-153.25	-6	-6	0	0
OH^-	-14.00	-1	0	0	0
$P_2O_6^{4-}$	-11.09	4	2	0	2
$Fe(OH)_2^+$	-18.69	-2	-1	1	0
$Fe(OH)_3$	-25.58	-3	-1	1	0
$Fe(OH)_4^-$	-34.62	-4	-1	1	0
$Fe_2(OH)_2^{+4}$	-28.99	-2	-2	2	0
$Fe_3(OH)_4^{+5}$	-45.36	-4	-3	3	0
$FeH_2PO_4^{2+}$	11.96	2	-1	1	1
$FeHPO_4^+$	4.76	1	-1	1	1
FeO_4^{2-}	-125.87	-8	-4	1	0
$FeOH^{2+}$	-15.21	-1	-1	1	0
$H_2P_2O_6^{2-}$	6.71	6	2	0	2
$H_2PO_2^-$	-15.01	6	4	0	1
$H_2P_2O_3^-$	2.69	4	2	0	1
$H_3P_2O_6^-$	9.27	7	2	0	2
$H_3P_2O_3$	4.19	5	2	0	1
HO_2^-	-71.25	-3	-2	0	0
$HP_2O_6^{3-}$	-0.72	5	2	0	2
H_3PO_2	-13.71	7	4	0	1
PH_3	-18.1	11	8	0	1
$PH_{3(g)}$	-16.63	11	8	0	1
Fe(c)	-16.097	0	2	1	0
$Fe(OH)_{2(c)}$	-12.996	-2	0	1	0
$Fe_3O_{4(c)}$	-37.077	-8	-2	3	0
$Fe_3(PO_4)_2{:}8H_2O(c)$	36	0	0	3	2
$Fe(OH)_{3(am)}$	-17.911	-3	-1	1	0
$Fe_2O_{3(cr)}$	-26.448	-6	-2	2	0
$Fe_3(OH)_{8(c)}$	-46.262	-8	-2	3	0
$FeOOH_{(cr)}$	-14.02	-3	-1	1	0
$FePO_4{:}2H_2O_{(c)}$	13.38	0	-1	1	1
$P_{(c)}$	-13.19	8	5	0	1

This may conduce to the formation of a large number of chemical species (see Table 1); therefore, it is very convenient to find out, at the experimental conditions, which are the thermodynamically most favoured species to be formed. In order to do this, we construct - using the software MEDUSA [12,13] with its thermodynamic constants database HYDRA - a Pourbaix-type diagram (E-pH), see Figure 1. For the construction of this E-pH diagram, 36 soluble and 10 solid species were considered along with the experimental conditions. Table 1 summarizes the data corresponding only to the most significant products.

Using the data shown in Figure 1 and the experimental pH (0.5) it is possible to construct the predominance zone diagram shown in Figure 2A. From it, one notes that in the system considered in this work, iron oxidation may produce two different soluble Fe (II) species and one insoluble Fe (III) solid phase, depending on the applied potential. At high potential values steel surface phosphatizing is favoured. It is important to mention that Ishihara and Asakura [8] have proposed that iron oxidation in 0.5 H_3PO_4 aqueous media containing H_2O_2 would produce γ–Fe_2O_3(c) however, form our thermodynamic study we can affirm that this is not feasible.

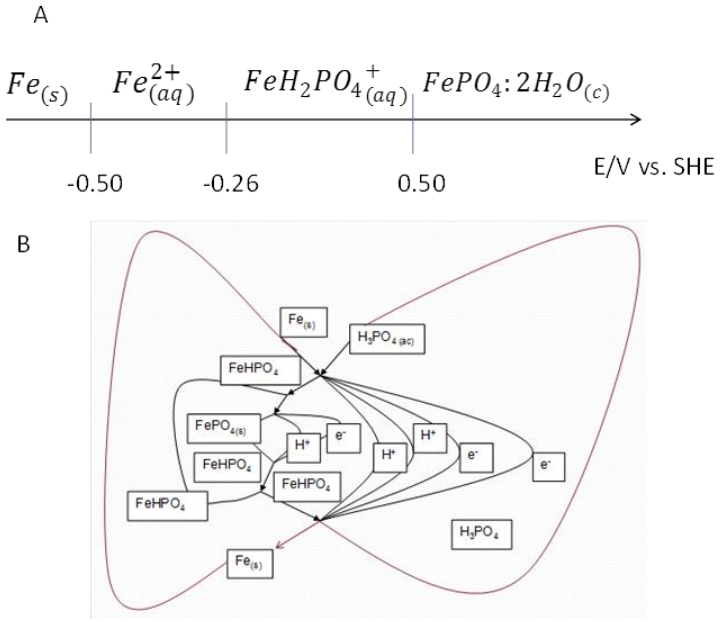

Figure 2. A. Theoretical predominant chemical species zone formed in the steel surfaces immersed in a concentrate H_3PO_4 aqueous solution as a function of the applied potential. B. Steel phosphatizing process represented by chemical operads.

3.2 Potentiodynamic oscillations

Figure 3 shows a typical CV recorded in the system steel/H_3PO_4 solution. It is possible to note the formation of a well-defined current peak, I, at around -50 mV during the forward, anodic segment, which could be related with the formation of soluble Fe (II) species, Fe^{2+} and $FeH_2PO_4{}^{+}$, followed by a second current peak, II, at around 250 mV due to formation of a passive corrosion layer on the steel surface mainly composed by $FePO_4{:}2H_2O_{(c)}$, see Figure 2. When 600 mV was reached, the scan

potential was inversed towards the cathodic direction. During this backward potential scan, current oscillations, CO, were clearly noted in the interval which goes from 530 to 300 mV.

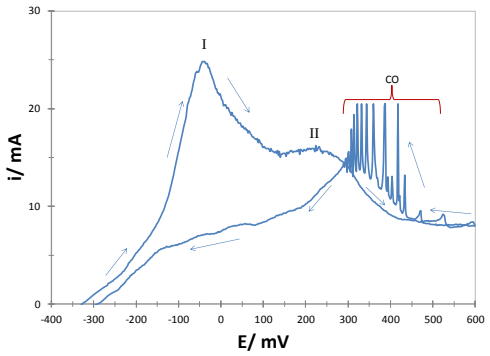

Figure 3. Experimental cyclic voltammetry recorded in the system steel/H_3PO_4 aqueous solution. The potential scan started at -400 mV in the positive direction, as arrows indicate, at a 4 mVs^{-1} sweep potential rate. The formation of two oxidation peak (I and II) during the forward potential scan and a current oscillation zone (CO) recorded during the backward potential scan in the cathodic direction are indicated in the figure.

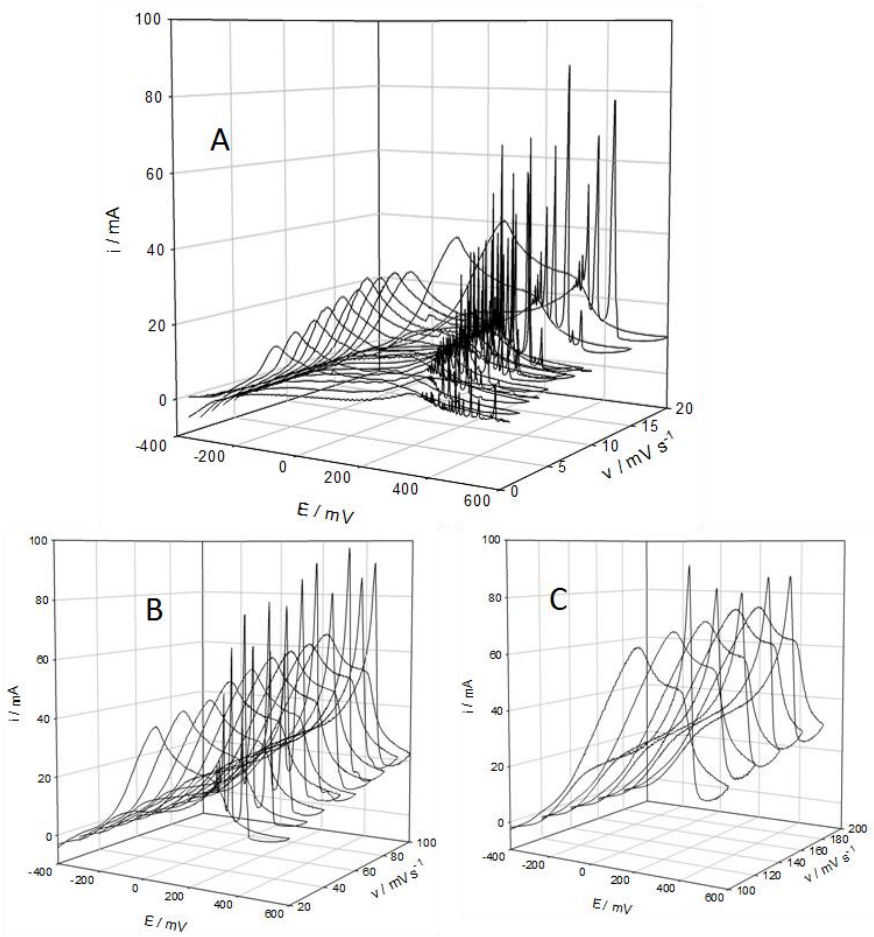

Figure 4. Experimental cyclic voltammetry families recorded in the system steel/H_3PO_4 aqueous solution at a different scan rates, low (A) medium (B) and high (C) range. In all cases the potential scan started at -400 mV in the positive direction.

3.2.1 Influence of the scan potential rate

Figure 4 show families of CVs recorded in the system steel/H_3PO_4 solution for different scan rate range namely: 0 to 20, Figure 3A, 20 to 100, Figure 3B, and 100 to 200 mVs^{-1}. From this figure it is possible to note that current oscillations strongly depends on the scan rate value however even for the heights values they are still present.

3.3 Potentiostatic oscillations

Figure 5 shows a typical experimental current transient recorded in the system steel/H_3PO_4 aqueous solution after imposing a double potential step as follows: first, a potential step from -400 to 600 mV (200 s), not shown, and a second potential step from 600 to 300 mV (200 s). During the first potential step, nucleation and growth of $FePO_4{:}2H_2O_{(c)}$, are involved, further discussion in this respect will be reported elsewhere [14]. During the second potential step current oscillations where recorded after about 30 s to be initiated the potential perturbation.

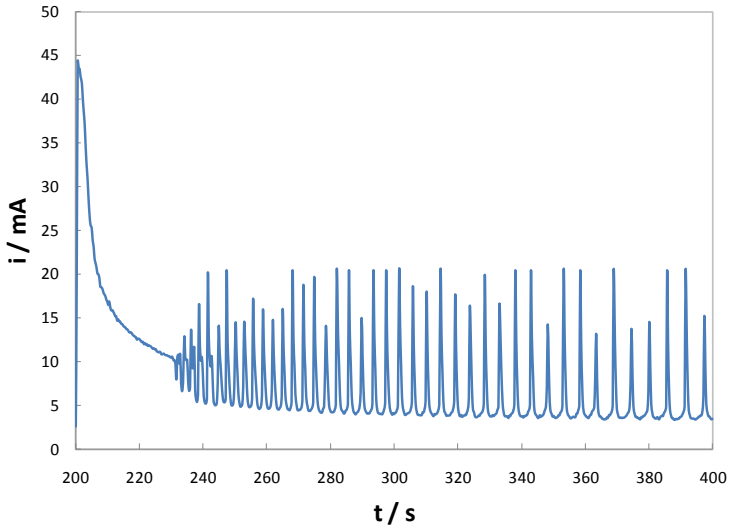

Figure 5. Typical experimental potentiostatic current transients recorded in the system steel/H_3PO_4 aqueous solution after imposing the following potential program: a potential step from -400 to 600 mV (200 s), not shown, and a second potential step from 600 to 300 mV (200 s).

3.3 SEM Analysis

Figure 6 shows a SEM image of the ASI SAE 1045 electrode surface before it was immersed in the H_3PO_4 aqueous solution, Figure 6a, and after immersion in the H_3PO4 aqueous solution and imposing a double potential step, alone with their corresponding EDX analysis.

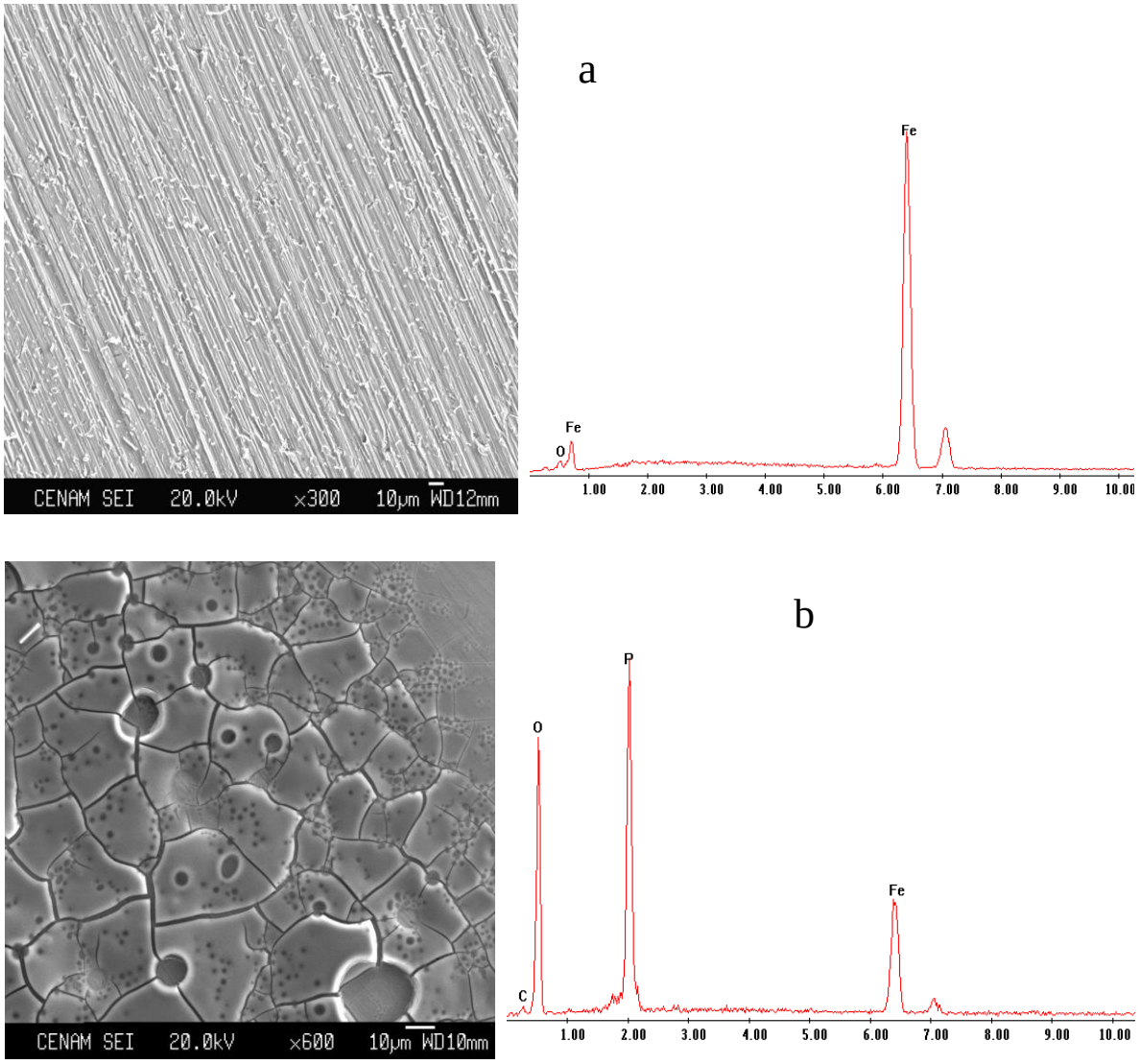

Figure 6. Secondary electron images and their corresponding EDX analyses of a) the bare steel surface and b) after immersion in the H_3PO4 aqueous solution and imposing a double potential step as follows: first potential step from -400 to 600 mV (200 s) and second potential step from 600 to 300 mV (200 s).

It is possible to note that the potential perturbation of the electrode produced on its surfaces well defined $FePO_4{:}2H_2O_{(c)}$ grains (fist potential step) and that multiple intergranular pits are formed during the second potential step.

3.4 Time Series Analysis.

3.4.1 Nonlinear System Dynamical Analysis

Chaos theory (as part of Nonlinear System Dynamic Analysis) has been frequently applied to the analysis of periodic, multiperiodic, chaotic and stochastic signals, bringing in several mathematical and graphical methods in order to define various parameters, and more precisely, metric properties

which allow additional means to construct a deeper understanding of the system under study. The present system, ASI SAE 1045 electrode immersed in H_3PO_4 aqueous solution, can be considered to be a dynamical system, for the physicochemical and electrochemical properties of this system evolves in time, and as such it may be specified by a set of variables, the state of which is described at any time by a set of specific values of these variables. This can be pictured by a point in the state space; the evolution of which or changes in the system which occur as a result of perturbations or of its tendency to reach local equilibrium, gives rise to trajectories in the state space. The plot that depicts these trajectories, namely, the evolution of the system from its initial conditions is called "attractor" [15-19]. The points making up the attractor of a time series $X(t_i)$ in a constructed phase space with dimension D_E can be generated by the following expression:

$$X(t_i) = \{(X(t_i), X(t_i + \tau))...X(t_i + (D_E - 1)\tau)\} \quad (1)$$

This procedure has been termed as the "time delay method", and it was used presently to generate the attractors for the electrochemical oscillations measured. In this case $X(t_i)$ was substituted by $I(t_i)$ the experimental current values, see Figures 5 and 7, gathered from the electrochemical experiments, and τ is the delay time which is a multiple of the sampling time Δt. D_E is the embedded dimension of the constructed phase space.

For the present system, the rate at which it approaches its attractor is given by a decay exponent for the dynamical system variables, such as the Lyapunov exponents, The Lyapunov exponent is a measure of the rate at which nearby trajectories in phase space diverge. Chaotic orbits have at least one positive Lyapunov exponent. For periodic orbits, all Lyapunov exponents are negative. If the ASI SAE 1045 / H_3PO_4 system behaves following a form fully at random, the attractors would show no recognizable structure and the Lyapunov exponents would be zero. If the system is undamped, the morphology of the attractor may look like a closed path in the state space, resembling an orbit or limit cycle.

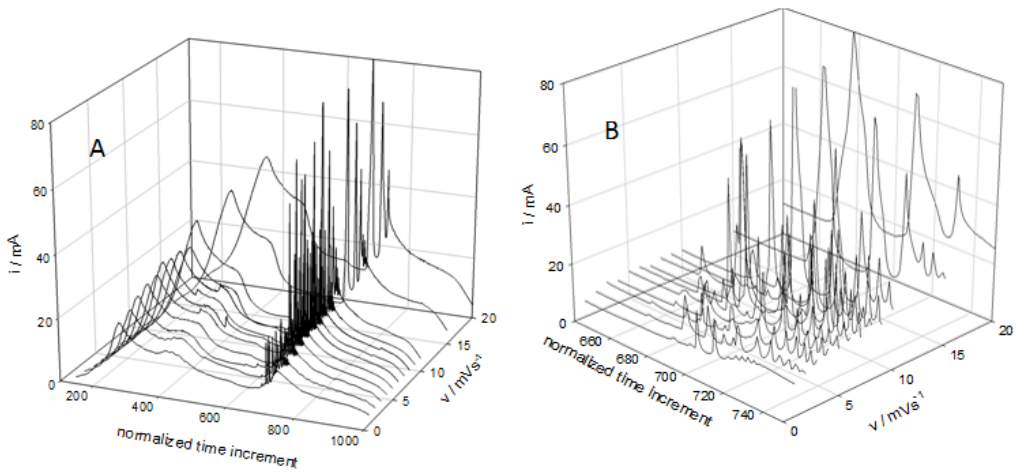

Figure 7. A. Normalized time series, as a function of the scan rate, recorded from potentiodynamic experiments, see Figure 4A. B. A close up view of the zone where current oscillations occurred.

In the expression above, D_E was taken to be 2, and after simplification, the phase space plot was constructed from the $I(t_i)$ data vs $I(t_i-\tau)$; Figure 8 presents the attractors generated in three dimensions as from the current time series obtained (see Figure 7B).

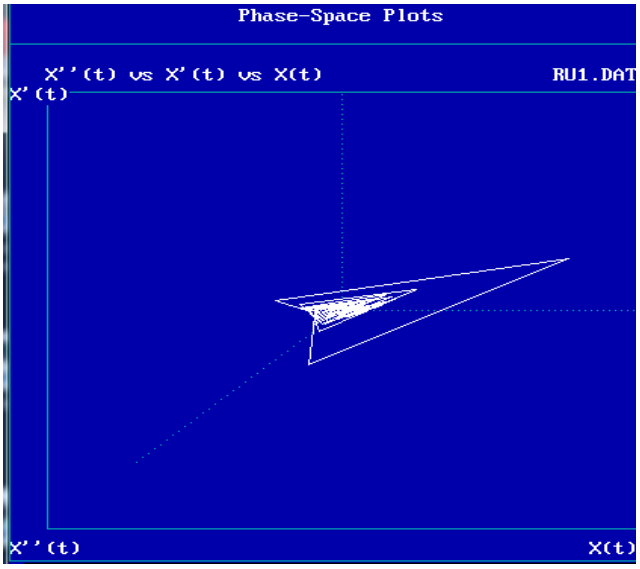

Figure 8. Concorde-like strange attractor generated for the current plot recorded at 1 mVs^{-1}, see Figure 7B, for the ASI SAE 1045 / H_3PO_4 system using the CHAOS DATA ANALYZER, CDA, program [20].

Table 2. Dynamical system variables calculated from time series shown in Figures 5 and 7B using the CHAOS DATA ANALYZER, CDA, program [20].

Scan rate /mVs-1	Lyapunov exponent	Capacity dimension	Correlation dimension
1	0.358	1.000	1.504
3	0.563	0.792	0.871
4	0.332	0.790	0.962
5	0.363	0.404	0.745
6	0.540	0.661	1.172
7	0.515	0.161	0.926
8	0.452	0.292	0.888
9	0.419	0.585	1.014
10	0.431	0.292	0.661
15	0.600	0.404	0.665
20	0.546	0.953	0.368
30	0.371	1.000	0.798
Potentiostatic See Figure 5	0.456	1.000	1.605

In the present case all the Lyapunov exponents were positive, see Table 2. This may be interpreted as rather a special case, because the trajectories taken by the system appear to diverge, though the behaviour is not quite random. Even if it cannot be absolutely predicted, is relevant to point out that this lack of predictability is intrinsic to the positive Lyapunov exponents. The inherent nature of the exponents, or their positive character, is practically related with the rate with which adjacent trajectories in the constructed phase space plot diverge. Thus, the attractors found for the present system are not simple (fixed points, limit cycles or a torus attractors); they are rather homoclinic strange attractors with non-integer fractal dimensions, as can be seen in Table 2 A dynamical system that behaves in this way is said to exhibit a chaotic behaviour, with a consequent fundamental long range unpredictability; considering that seven days for this system can be assumed as such, and sensitivity to very small variations in its initial conditions.

The capacity dimension (also called the Hausdorff dimension) is calculated by successively dividing the phase space with embedding dimension D_E into equal hypercubes and plotting the log of the fraction of hypercubes that are occupied with data points versus the log of the normalized linear dimension of the hypercubes, the values calculated for the present study are also reported in Table 2. The correlation dimension is taken as the average slope of the cumulative curve over the middle one-quarter of the vertical scale, and the error is taken as half the difference of the maximum and minimum slope over the same range. The CDA program calculates embedding dimensions between 1 and 10. The correlation dimension is supposed to be more reliable than the capacity dimension for data of high dimension, but the calculation time to process all the data points is much longer. However, a good estimate is usually obtained from only the first few points. A dimension greater than about five implies essentially random data.

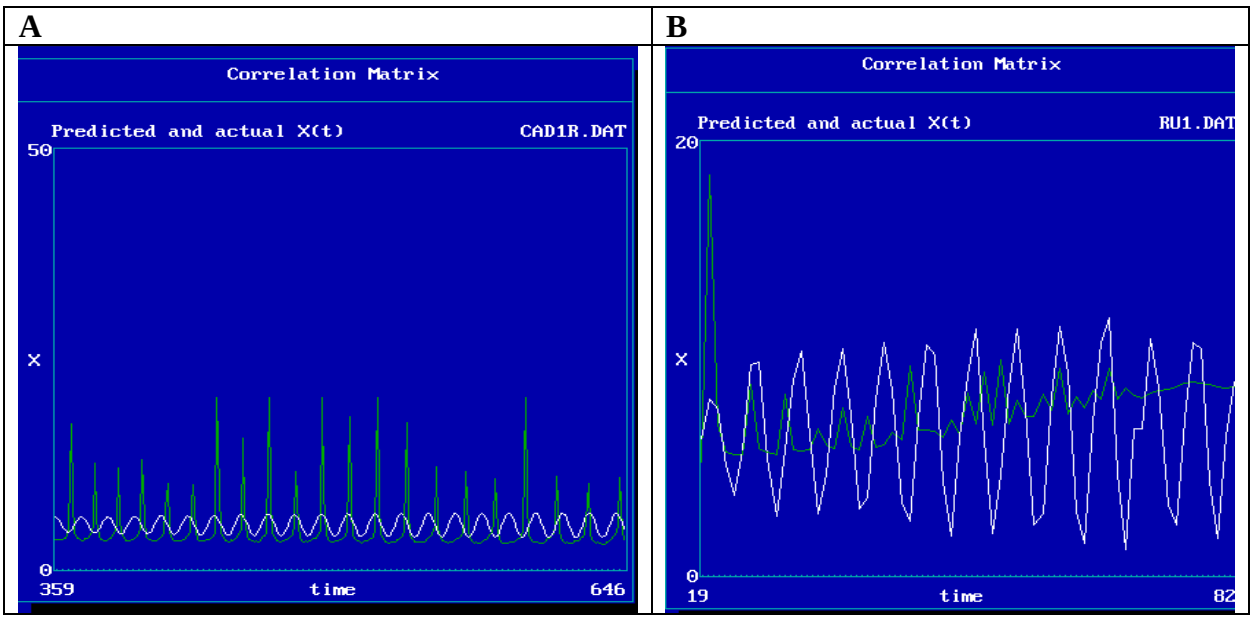

Figure 9. Comparison of predicted (white line) and experimental (green line) time series recorded from potentiostatic (A) and potentiodynamic (B) experiments. The theoretical plots were calculated with the corresponding correlation matrix using the CHAOS DATA ANALYZER, CDA, program [20].

The correlation matrix, which is a two-dimensional (M X M) matrix formed by putting the value of the correlation function with tau=0 along the diagonal and putting the value of the correlation function with tau=1 to the right and left of the diagonal and then tau=2, and so forth until the matrix is filled may be used to simulate the experimental data, see Figure 9. The data are fitted to a linear superposition of the first three eigenfunctions. The model equations can be used to predict the next 18 values in the time series. If the data consist of chaotic and random components, this procedure should help extract the chaos from the randomness. The number of significant eigenvalues, like the correlation dimension, see Table 2, is a measure of the complexity of the system.

3.4.2 Recurrence analysis

A number of methods have been devised to compute dynamical parameters from time series [18]. Such parameters are the information dimension, entropy, Lyapunov exponents, dimension spectrum, etc. In all cases it is assumed that the time series is obtained from an autonomous dynamical system, i.e. the evolution equations do not contain the time explicitly. It is also assumed that the time series is much longer than the characteristic times of the dynamical system. Eckmann et al [19] have described a new diagnostic (graphical) tool for measuring the time constancy of dynamical systems, which they call recurrence plot. This tool tests the above assumptions, and gives useful information also when they are not satisfied. The information obtained from recurrence plots is often surprising, and not easily obtainable by other methods.

Let *x(i)* be the *i*-th point on the orbit describing a dynamical system in *d*-dimensional space, for $i = 1, ..., \boldsymbol{N}$. The recurrence plot is an array of dots in a $\boldsymbol{N}$ x $\boldsymbol{N}$ square, where a dot is placed at *(i,j)* whenever *x (j)* is sufficiently close to *x(i).* In practice one proceeds as follows to obtain a recurrence plot from a time series $\{u_i\}$. First, choosing an embedding dimension *d,* one constructs the *d*-dimensional orbit of *x(i)* by the method of time delays *(i.e.* if the u_i are scalar, $x(i) = (u_i, u_{i+1}, \ldots, u_{i+d-1})$). Next, one chooses *r(i)*such that the ball of radius $r(i)$ centered at $x(i)$ in R^d contains a reasonable number of other points $x(j)$ of the orbit. In our computation analysis, see below, we have allowed the radius $r(i)$ to depend on the point $x(i)$, and $r(i)$ has been selected by a routine used in our algorithm for the determination of the Lyapunov exponents. Finally, one plots a dot at each point (i, j) for which $x(j)$ is in the ball of radius $r(i)$ centered at $x(i)$. We call this picture a *recurrence plot.*

Note that the *i, j* are in fact 'quantized' times, in the sense that they are integer times: therefore a recurrence plot describes natural (but subtle) time correlation information. Recurrence plots tend to be fairly symmetric with respect to the diagonal $i = j$ because if $x(i)$ is close to $x(j)$, then $x(j)$ is close to $x(i)$. There is, however, no complete symmetry because we do not require $r(i) = r(j)$**.**

Fig.10 (a,b,c) shows different potentiodynamic experimental time series of 'rectified' voltammograms with their corresponding recurrence plots at low (A), media (B) and high scan rates. What one observes in Fig.10a is a current oscillation (CO) zone which in the recurrence plot appears as a series of crossed lines approximately between the range going from 607 to 745 (unit times). In the same recurrence plot; sections of parallel lines forming crossed lines could be considered as Cantor-like fractal patterns.

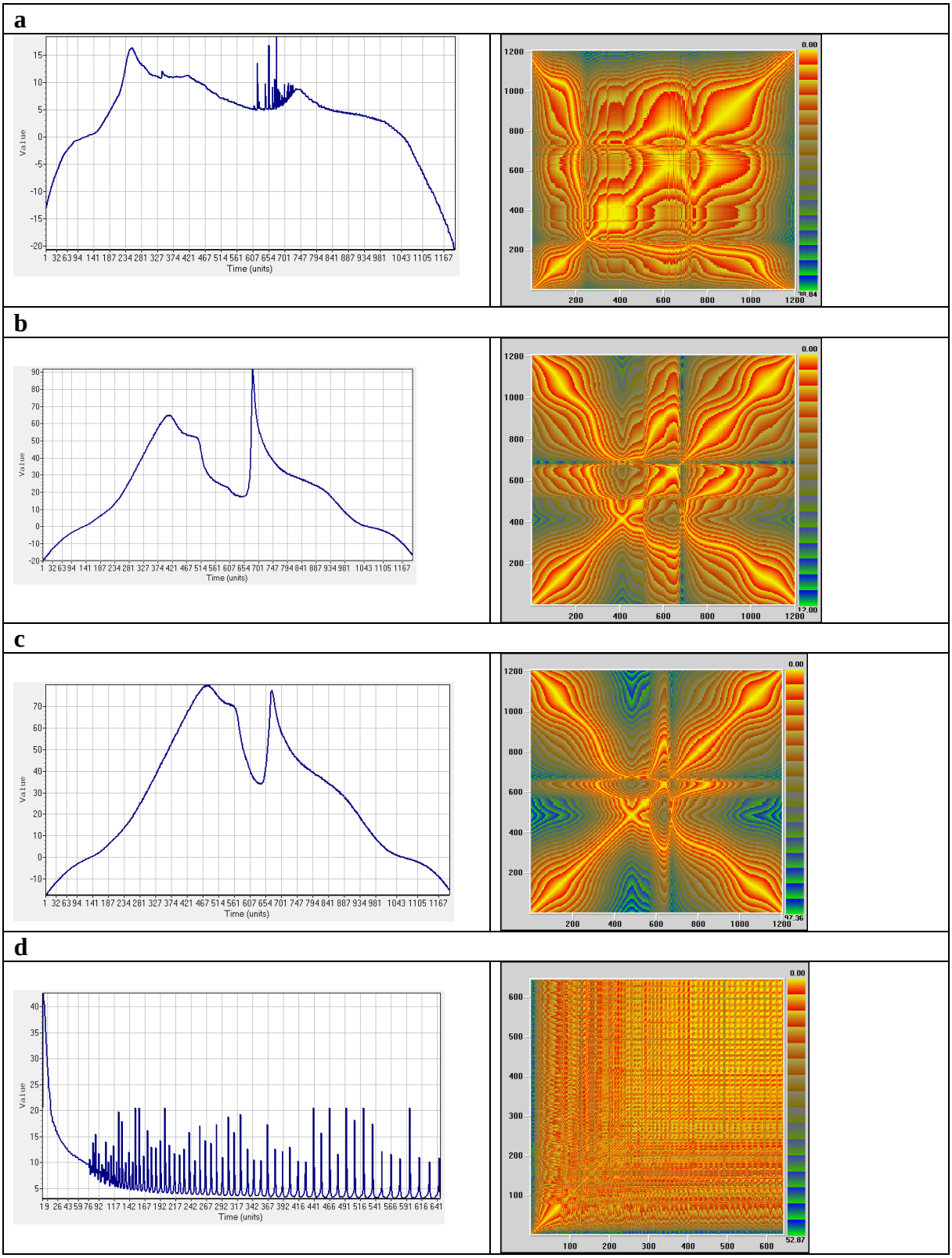

Figure 10. Experimental time series recorded during potentiodynamic experiments, in different scan rate range, low (A), media (B), high (C), see Figure 4, and potentiostatic (d), see Figure 5, electrochemical experiments with their corresponding recurrence plots obtained with VISUAL RECURRENCE ANALYSIS SOFTWARE [21].

In figures 10b and 10c one can see some very pronounced peaks which in the corresponding recurrence plots appear as single crossed lines (in blue). In none of figures 10b and 10c there is visual evidence of complex fractal patterns; what one observes there, are 'ghosts' resulting from combinations of tetrads of paraboloids or couples of hyperboloids which are typical of recurrence plots formed from signals in which one has Gaussian-like or Lorentzian–like peaks; this is very often the case during the analysis of electroanalytical signals. Fig.10d shows another view (compared with Fig.5) of the resulting double step chronoamperogram (for the second potential step only) with its corresponding recurrence plot calculated with a value of the embedded dimension equal to 2 (calculated with the false nearest neighbors method) and a lag time of 3 (this value has been obtained from a mutual information calculation). Besides, as has been said for the double step chronoamperogram of Fig. 5, the attractor generated in Fig. 8 is a strange attractor with an integer-like fractal dimension of 1.504 (less than 5 and therefore not indicative of random behavior); which means that for a scan rate of 1 mVs^{-1} the number of variables and ordinary differential equations (ODE's) that could be set to model that particular system is between 2 and 2* 1.504 + 2 = 5 variables or ODE's. The fact that the largest positive Lyapunov exponent for that scan rate (1 mVs^{-1}) is 0.358 (see Table 2) is indicative of chaotic behavior; but this is not solely a criterion of chaoticity, for it is well-known that noise added to a non-chaotic time series can also generate positive Lyapunov exponents. Fortunately, one has some other parameters or metric properties that can be calculated to find out chaotic behavior; among them, the spatiotemporal entropy for the signal of Fig. 10d resulted in a value of 69% which corresponds to chaotic behavior. On the other hand, the recurrence plot corresponding to the potentiodynamic transient signal of Fig. 10d exhibits a combination of fractal patterns (typical of chaotic behavior) with patterns which one could associate to quasi-periodic-like behavior. Up to our knowledge, there are unfortunately no developed methods of nonlinear signal analysis in which one can detect and classify mixed types of dynamical behaviors; so we restricted ourselves to the usual classification in chaos theory of nonlinear dynamical systems as: Periodic, multiperiodic, chaotic and stochastic.

4. CONCLUSIONS

For the first time current oscillations are reported and characterized in the system ASI SAE 1045 electrode immersed in H_3PO_4 aqueous solution, we found out evidence of chaotic behavior during the process of electrochemical phosphating of ASI SAE 1045 steel. This evidence was supported through the calculation of some metric properties like correlation dimensions (approximately equal to fractal dimensions), which led to the conclusion that for low scan rates (for instance 1 mVs^{-1}) the 'complexity' of the system measured in terms of the number of variables and ODE's necessary to model and simulate it, is between 2 and 5. On the other hand, the largest Lyapunov exponents calculated for this system resulted to be positive; the spatiotemporal entropy, as we saw above, was indicative of chaotic behavior. Finally, from the geometrical standpoint: the homoclinic attractors generated in state space have shown a Concorde-like recognizable structure (i.e.

not random) and the recurrence plot have also shown fractal structure corresponding to the electrochemical oscillations in the electrochemical signals.

ACKNOWLEDGMENTS

G.A. Vázquez-Coutiño (a member of ISSCultArt: International Society of Science Culture and Arts) dedicates this work to the memory of my friend Prof. E. Lacomba, who has recently passed away and was perhaps the most important and influential expert in Nonlinear System Dynamic Analysis and Chaos Theory in Mexico. M.P.P. and M.R.R. thanks CONACYT for Project Nos. 24658 ("Nucleación y crecimiento electroquímico de nuevas fases") and 22610714. Also M.P.P., M.T.R.S., H.H.H. and M.R.R. gratefully thank the SNI for the distinction of their membership and the stipend received. M.R.R. and M.P.P. wish to thank Departamento de Materiales, UAM-A, for financial support given through Projects of "Area Ingeniería de Materiales". This work was done in partial fulfillment of GAVC's Ph.D. requirements.

References

1. D. Sazou, *Electrochim. Acta*, 42 (1997) 627-637.
2. I. Z. Kiss and V. Gáspár, L. Nyikos, P. Parmananda, *J. Phys. Chem. A*, 101, (1997) 8668-8674
3. A. G. Cioffi, R. Scott Martin, I. Z. Kiss, *J. Electroanal. Chem*. 659 (2011) 92–100.
4. M. Fleishmann, M. Labram, C. Gabrielli, *J. Electroanal. Chem*. 150 (1983) 111–123.
5. K. Ogura, W. Lou, M. Nakayama, T. Fukume, *J. Electroanal. Chem.* 441 (1998) 191-195.
6. E. Cazares-Ibáñez, G.A. Vázquez-Coutiño, E. García-Ochoa, *J. Electroanal. Chem*. 583 (2005) 17–33.
7. A.Eftekhari, *Physics Letters A*, 332 (2004),382-388
8. A. Ishihara, S. Asakura *Sensor and Actuators A*, 39 (1993) 231-235.
9. F. Argoul, J. Huth, P. Merzeau, A. Arnrodo, H.L. Swinney, *Physica D*, 62 (1993) 170-185.
10. W. Li, K. Nobe, A.J. Pearlstein, *J. Electrochem. Soc*. 140 (1993) 721-728.
11. M. Hashimoto, S. Miyajima, T. Murata, *Corros. Sci*. 33 (1992) 905-915.
12. Puigdomenech, I. MEDUSA (Making Equilibrium Diagrams Using Sophisticated Algorithms), http://www.kemi.kth.se/medusa/.
13. A. Hernández-Espejel, M. Palomar-Pardavé, R. Cabrera-Sierra, M. Romero-Romo, M.T. Ramírez-Silva, E.M. Arce-Estrada, Kinetics and Mechanism of the Electrochemical Formation of Iron Oxidation Products on Steel Immersed in Sour Acid Media, *J. Phys. Chem. B*, 115 (2011) 1833–1841.
14. M. Palomar-Pardavé, G. Vazquez-Coutiño, M. Romero Romo, M.G. Montes de Oca-Yemha, M.T. Ramírez-Silva, *J. Solid. State. Electrochem*. (2012) DOI 10.1007/s10008-012-1882-5.
15. A. Legat, V. Dolecek, *J. Electrochem. Soc*., 142 6 (1995) 142.
16. J. Stringer, J. Markworth *Corros, Scien*., 35 (1993) 1.
17. J.P. Eckmann, *Rev. Mod. Phys*. 57 (1985) 617.
18. J.P. Eckmann, *Rev. Mod. Phys*. 53 (1981) 643.
19. J.P. Eckmann, S.Oliffson Kamphorst. D. Ruelle *Europhys. Lett*., 4 (1987) 973-977.
20. Chaos Data Analyzer program, IBM PC Version 1.0 (c) 1992 by J.C. Sprott, University of Wisconsin, Madison, WI 53706.
21. Visual Recurrence Analysis Software, version 4.7, Copyright (C) 1996-2004 Eugene Kononov.